SPODI

High-resolution powder diffractometer

M. Hoelzel, A. Senyshyn, V. Baran, M.J. Mühlbauer

Forschungsneutronenquelle Heinz Maier-Leibnitz (FRM II)
Technische Universität München

Contents

1. **Applications of neutron powder diffraction**

Powder diffraction reveals information on the phase composition of a sample and the structural details of the phases. In particular, the positions of the atoms (crystallographic structure) and the ordering of magnetic moments (magnetic structure) can be obtained. In addition to the structural parameters, also some information on the microstructure (crystallite sizes/microstrains) can be obtained. The knowledge of the structure is crucial to understand structure – properties – relationships in any material. Thus, neutron powder diffraction can provide valuable information for the optimisation of modern materials.

Typical applications:

Material	**Task**
lithium-ion battery materials	positions of Li atoms, structural changes/phase transitions at the electrodes during operation, diffusion pathways of Li atoms
hydrogen storage materials	positions of H atoms, phase transformations during hydrogen absorption/desorption
ionic conductors for fuel cells	positions of O/N atoms, thermal displacement parameters of the atoms and disorder at different temperatures, diffusion pathways of O/N atoms
shape memory alloys	stress-induced phase transformations, stress-induced texture development
materials with collosal magneto resistance effect	magnetic moment per atom at different temperatures
catalysers	structural changes during the uptake of sorbents
piezoelectric ceramics	structural changes during poling in electric field, positions of O atoms
nickel superalloys	phase transformations at high temperatures, lattice mismatch of phases
magnetic shape memory alloys	magneto-elastic effects, magnetic moment per atom at different temperatures and magnetic fields

2. Basics of Powder Diffraction

Diffraction can be regarded as detection of interference phenomena resulting from coherent elastic scattering of neutron waves from crystalline matter. Crystals can be imagined by a three-dimenional periodic arrangement of unit cells. The unit cell is characterised by the lattice parameters (dimensions and angles) and the positions of atoms or molecules inside the unit cell.
For diffraction experiments the probe should have a wavelength comparable to interatomic distances: this is possible for X-rays (synchrotron radiation), electrons or neutrons.

Structure factor

The structure factor describes the intensity of Bragg reflections with Miller indexes (*hkl*), based on the particular arrangement of all atoms *j* in the unit cell

$$F_{hkl} = \sum_{j=1}^{n} b_j T_j \exp\left\{2\pi i \vec{H}\vec{R}_j\right\}$$

where
F_{hkl}: structure factor of Bragg reflection with Miller indexes *hkl*.
n: number of atoms in unit cell
$b_{j:}$ scattering lengths (in case of neutron scattering) or atomic form factor (in case of X-ray diffraction) of atom *j*
$T_{j:}$ Debye Waller factor of atom *j*

The scalar product $\vec{H}\vec{R}_j$ consists of the reciprocal lattice vector $\vec{H}$ and the vector $\vec{R}_j$, revealing the fractional atomic coordinates of atom j in the unit cell.

$$\vec{H}\vec{R}_j = \begin{pmatrix} h \\ k \\ l \end{pmatrix} \cdot \begin{pmatrix} x_j \\ y_j \\ z_j \end{pmatrix} = hx_j + ky_j + lz_j$$

Thus, the structure factor can also be given as follows:

$$F_{hkl} = \sum_{j=1}^{n} b_j T_j \exp 2\pi i\left\{hx_j + ky_j + lz_j\right\}$$

The intensity of a Bragg reflection is proportional to the square of the absolute value of the structure factor: $I \propto \left|F_{hkl}\right|^2$

Debye-Waller Factor

The Debye-Waller Factor describes the decrease in the intensity of Bragg reflections due to atomic thermal vibrations.

$$T_j(Q) = \exp\left\{-\frac{1}{2}\left\langle\left(\vec{Q}\vec{u}_j\right)\right\rangle\right\}$$

vector $\boldsymbol{u_j}$ reflects the thermal displacements of atom j

Braggs' Law

Braggs' Law provides a relation between distances of lattice planes with Miller indexes *hkl*, i.e. d_{hkl}, and the scattering angle 2θ of the corresponding Bragg peak. Braggs' law can be illustrated in a simplified picture of diffraction as reflection of neutron waves at lattice planes (Fig. 1). The waves which are reflected from different lattice planes interfere. We get constructive interference, if the path difference between the reflected waves corresponds to an integer multiple of the wavelength.
The condition for constructive interference (= Braggs' law) is then:

$$2d_{hkl}\sin\theta = n\lambda$$

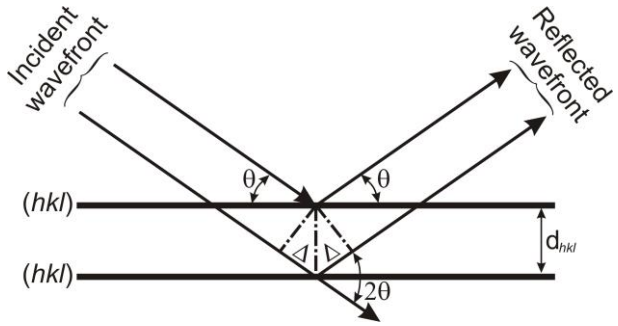

Figure 1: Illustration of Bragg's law: constructive interference of neutron waves, reflected from lattice planes, where θ, 2θ are Bragg angles, $2\Delta=2d_{hkl}\sin\theta$ is the path difference and $2\Delta=n\lambda$ is the constructive interference.

Applying Bragg's law one can derive the lattice spacings ("d-values") from the scattering angle positions of the Bragg peaks in a constant-wavelength diffraction experiment. With the help of d-values a qualitative phase analysis can be carried out.

Ewald's sphere

The Ewald's sphere provides a visualisation of diffraction with help of the reciprocal lattice. At first, we introduce the scattering vector ***Q*** and the scattering triangle (Figure 2). The incident neutron wave is described by a propagation vector $\boldsymbol{k_i}$, the scattered wave is given by $\boldsymbol{k_f}$. In the case of elastic scattering (no energy transfer) both vectors $\boldsymbol{k_i}$ and $\boldsymbol{k_f}$ have the same length which is reciprocal to the wavelength.

$$\left|\vec{k}_i\right| = \left|\vec{k}_f\right| = \frac{2\pi}{\lambda}$$

remark:

The length of the wave vectors are sometimes given as $\left|k_i\right| = \left|k_f\right| = \frac{1}{\lambda}$ *(This definition is found esp. in crystallographic literature, while the other one is more common for physicists).*

The angle between vectors $\boldsymbol{k_i}$ and $\boldsymbol{k_f}$ is the scattering angle 2θ. The scattering vector ***Q*** is the given by the difference between $\boldsymbol{k_i}$ and $\boldsymbol{k_f}$:

$$\boldsymbol{Q} = \boldsymbol{k_f} - \boldsymbol{k_i} \quad |Q| = 4\pi \frac{\sin\theta}{\lambda}$$

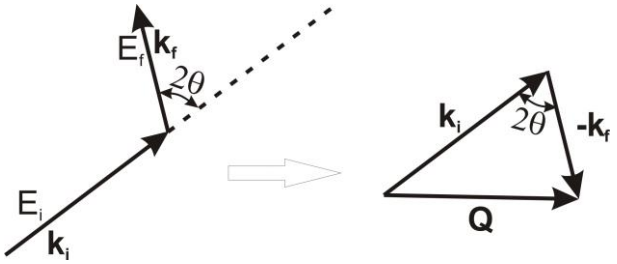

Figure 2: Illustration of scattering vector and scattering angle resulting from incident and scattered waves.

In the visualisation of the diffraction phenomena by Ewald the scattering triangle is implemented into the reciprocal lattice of the sample crystal – at first, we consider diffraction at a single crystal (Figure 3). Note that the end of the incident wave vector coincides with the origin of the reciprocal lattice. Ewald revealed the following condition for diffraction: we have diffraction in the direction of $\boldsymbol{k_f}$, if its end point (equivalently: the end point of scattering vector ***Q***) lies at a reciprocal lattice point *hkl*. All possible $\boldsymbol{k_f}$, which fulfil this condition, describe a sphere with radius $2\pi/\lambda$, the so called Ewald's sphere. Thus we obtain a hkl reflection if the reciprocal lattice point hkl is on the surface of the Ewald's sphere.

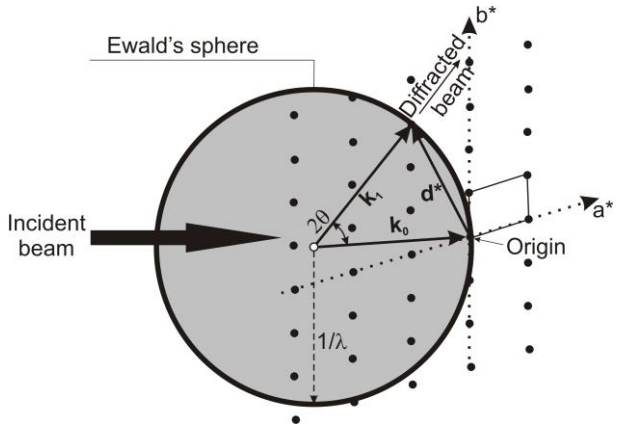

Figure 3: Illustration of diffraction using the Ewald's sphere (in crystallographic notation).

Here, the radius of Ewald's sphere is given by 1/λ (For $|k_i| = \frac{2\pi}{\lambda}$ we obtain a radius of 2π/λ).

We receive the following condition for diffraction: the scattering vector ***Q*** should coincide with a reciprocal lattice vector $\boldsymbol{H_{hkl}}$ (* 2π):

$$\vec{Q} = 2\pi\vec{H}_{hkl};\ \vec{H}_{hkl} = h\vec{a}^{\,x} + k\vec{b}^{\,x} + l\vec{c}^{\,x};\ \left|\vec{H}_{hkl}\right| = d^{x}_{hkl} = \frac{1}{d_{hkl}}$$

From this diffraction condition based on the reciprocal lattice we can derive Bragg's law:

$$\left|\vec{Q}\right| = 2\pi\left|\vec{H}_{hkl}\right| \rightarrow 4\pi\frac{\sin\theta}{\lambda} = \frac{2\pi}{d_{hkl}} \rightarrow 2d_{hkl}\sin\theta = \lambda$$

The Ewald's sphere is a very important tool to visualize the method of single crystal diffraction: At a random orientation of a single crystalline sample a few reciprocal lattice points might match the surface of Ewald's sphere, thus fulfil the condition for diffraction. If we rotate the crystal, we rotate the reciprocal lattice with respect to the Ewald's sphere. Thus by a stepwise rotation of the crystal we receive corresponding reflections.

Powder Diffraction in Debye-Scherrer Geometry

In a polycrystalline sample or a powder sample we assume a random orientation of all crystallites. Correspondingly, we have a random orientation of the reciprocal lattices of the crystallites. The reciprocal lattice vectors for the same *hkl*, i.e. $\boldsymbol{H_{hkl}}$, describe a sphere around the origin of the reciprocal lattice. In the picture of Ewald's sphere we observe diffraction effect, if the surface of the Ewald's sphere intersects with the spheres of $\boldsymbol{H_{hkl}}$ vectors. For a sufficient number of crystallites in the sample and a random distribution of grain orientations, the scattered wave vectors $\boldsymbol{k_f}$ describe a cone with opening angle 2θ with respect to the inident beam $\boldsymbol{k_i}$.
In the so called Debye-Scherrer Geometry a monochromatic beam is scattered at a cylindrical sample (Fig. 4). The scattered neutrons (or X-rays) are collected at a cylindrical detector in the scattering plane. The intersection between cones (scattered neutrons) and a cylinder (detector area) results in segments of rings (= Debye-Scherrer rings) on the detector (Fig 5). By integration of the data along the Debye-Scherrer rings one derives the conventional constant-wavelength powder diffraction pattern, i.e. intensity as a function of the scattering angle 2θ.

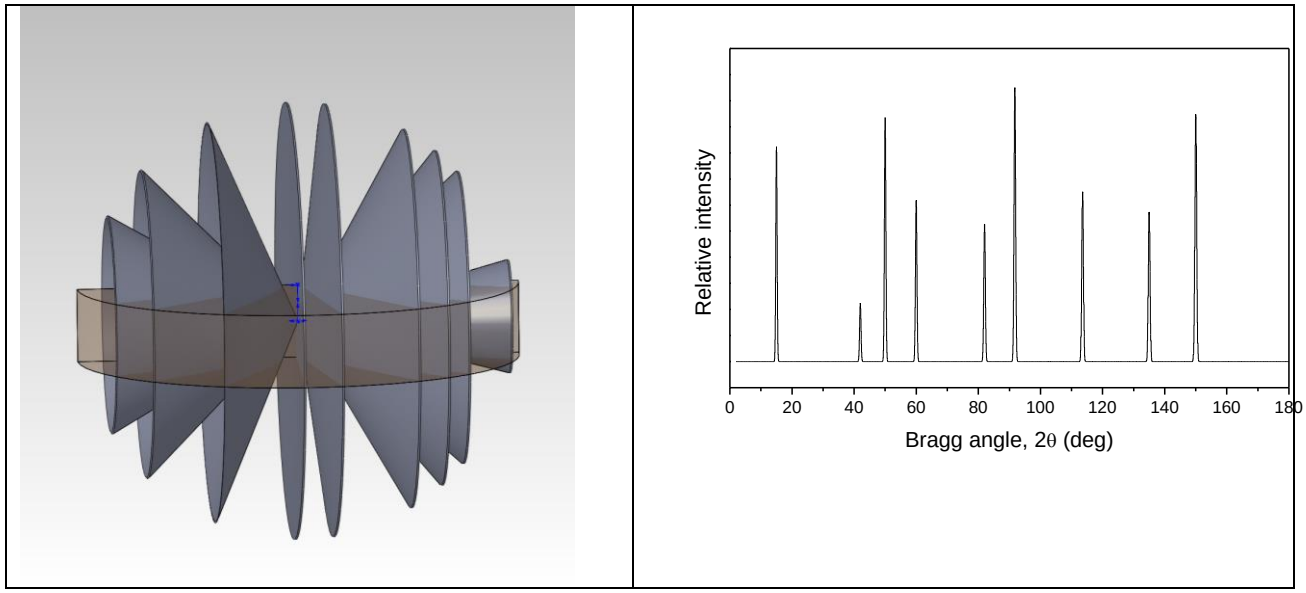

Figure 4: Illustration of powder diffraction in Debye-Scherrer geometry. On the left: cones of neutrons scattered from a polycrystalline sample are detected in the scattering plane. On the right: resulting powder diffraction pattern (after data integration along the Debye-Scherrer rings).

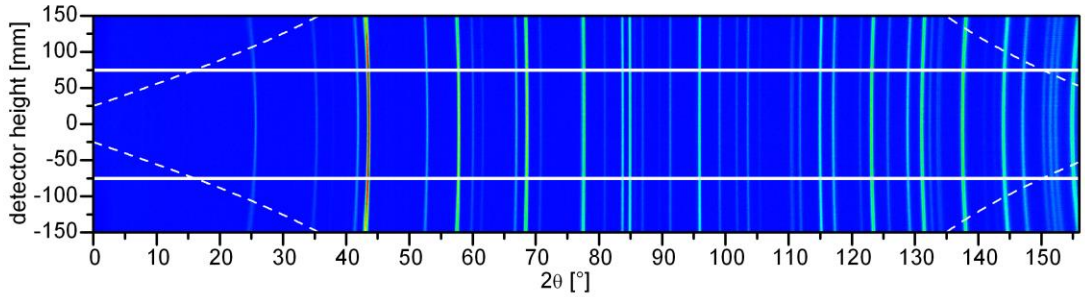

Figure 5: Two dimensional diffraction data (detector height vs. scattering angle 2θ), collected at high-resolution powder diffractometer SPODI, illustrating the Debye-Scherrer rings of a corundum sample.

Relations between Bragg positions and lattice parameters

With the help of Braggs law one can derive the lattice spacings “d-values” directly from the positions of Bragg reflections. The d-values are related with the lattice parameters of the unit cell (the cell dimensions *a,b,c* and the cell angles α,β,γ) and the Miller indexes (hkl) of the corresponding reflections. In the following, the relations are provided for the different crystal systems.

cubic $$\frac{1}{d_{hkl}} = \frac{h^2 + k^2 + l^2}{a^2}$$

hexagonal $$\frac{1}{d_{hkl}} = \frac{4}{3}\frac{h^2 + hk + k^2}{a^2} + \frac{l^2}{c^2}$$

tetragonal $$\frac{1}{d_{hkl}} = \frac{h^2 + k^2}{a^2} + \frac{l^2}{c^2}$$

orthorhombic $$\frac{1}{d_{hkl}} = \frac{h^2}{a^2} + \frac{k^2}{b^2} + \frac{l^2}{c^2}$$

monoclinic $$\frac{1}{d_{hkl}} = \frac{h^2}{a^2 \sin^2\beta} + \frac{k^2}{b^2} + \frac{l^2}{c^2 \sin^2\beta} + \frac{2hl\cos\beta}{ac\sin^2\beta}$$

3. Information from powder diffraction experiments

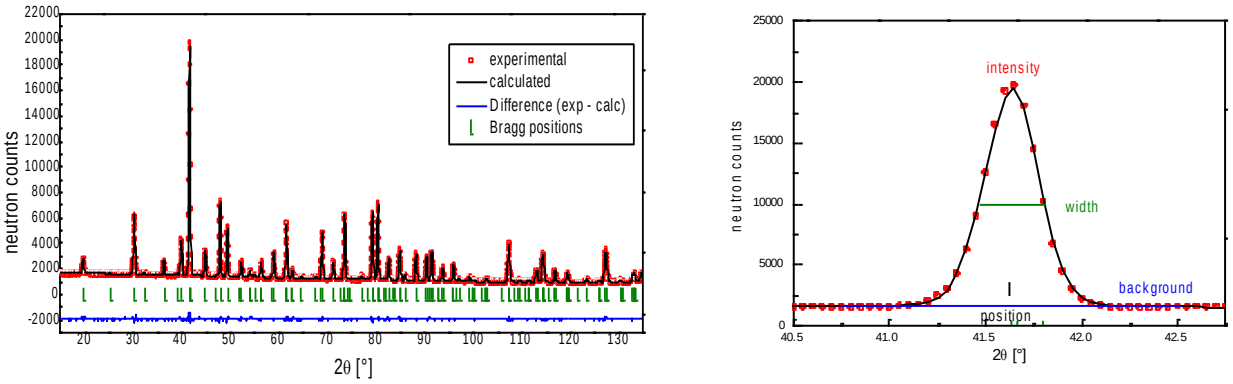

Figure 6: on the left: typical powder diffraction pattern. On the right: zoom on a single Bragg peak.

In the following, we will consider the information which can be derived from different elements of the diffraction patterns.

Positions (scattering angles) of Bragg reflections

- phase identification (from d-values)
- lattice parameters
- symmetry information (space group) by lattice parameters and selection rules (systematic extinction of reflections)

Intensity of Bragg reflections

- crystallographic structure
  - positions of atoms (fractional atomic coordinates)
  - occupancies of atoms on their sites
  - thermal displacement parameters
- magnetic structure
  - magnetic lattice (propagation vector)
  - magnetic symmetry (space group)
  - magnetic moment per atom
- quantitative phase analysis
- preferred orientation effects

Profiles of reflections

The reflection profiles result in a convolution of the instrumental resolution function with broadening effects of the sample

- microstructural information
  - microstrains
  - crystallite sizes

Modulation/Profile of Background

- short range order
- disorder
- amorphous contents

4. Evaluation of Powder Diffraction Data

The methods of data treatment can be classified in analysis of phase composition or phase transformation, structure solution and structure refinement.
Qualitative phase analysis is based on the determination of d-values and relative intensities (in particular intensities of strong reflections have to be considered). The phase identification is supported by crystallographic data bases (ICDD, ISCD), literature data and information from other methods (for instance, analysis of the chemical composition). Such kind of phase analysis is however typically carried out with X-ray diffraction.
The majority of neutron powder diffraction studies is based on experiments at various temperatures to investigate phase transformation behaviour as a function of temperature. There is an increasing demand for parametric studies, i.e. diffraction studies under various environmental conditions (temperature, electric or magnetic field, mechanical stress, gas atmosphere...) with particular attention to reaction pathways/reaction kinetics. This kind of investigations require in general high-intensity powder diffraction.
Powder diffracton data can be used both for phase identification and the refinement of structural parameters, such as lattice parameters, fractional atomic coordinates, atomic occupancies and atomic displacement parameters by the full profile Rietveld analysis. In the Rietveld method, the full diffraction pattern is calculated based on a structure model, taking into account the above mentioned structural parameters, as well as reflection profile parameters, instrumental parameters and background parameters. Using least-squares method, a stepwise refinement of the model parameters is carried out to describe (“to fit”) the experimental data.
Powder diffractometers are often classified as “high-resolution” or “high-intensity” diffractometers. High-resolution powder diffractometers are designed for structure refinements on complex systems. High-intensity diffractometers allow fast kinetic measurements to investigate phase transitions or chemical reactions.
Besides structure refinement, also structure solution can be done based on powder diffraction patterns by various methods.

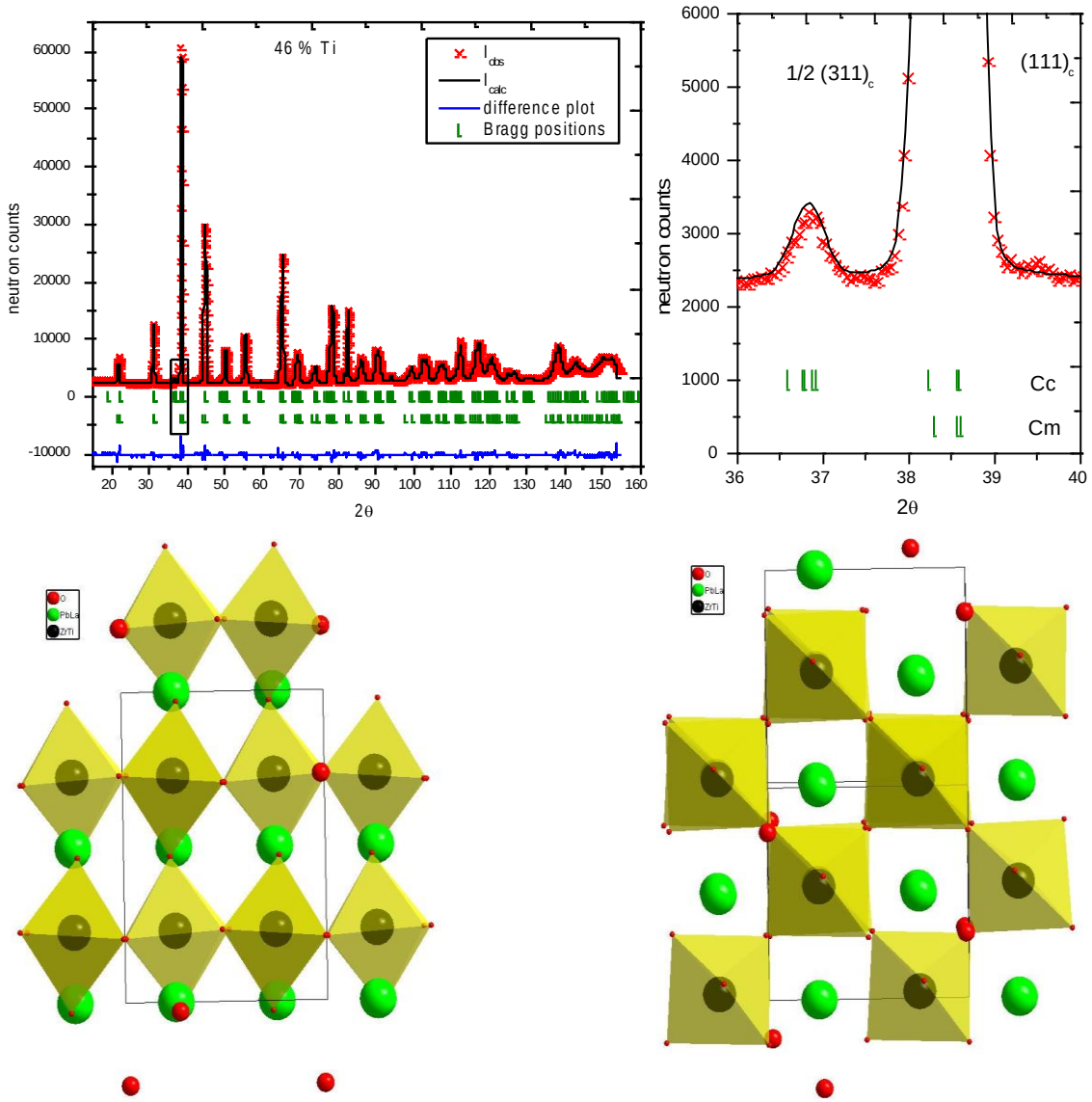

Figure 7: a) Data treatment of a measurement on the ferroelectric $Pb_{0.99}La_{0.01}Zr_{0.54}Ti_{0.46}O_3$, carried out at 5 K at diffractometer SPODI (FRM II): Diffraction pattern including experimental data, calculated data by Rietveld fit, Bragg reflection positions of the phases (space groups C_C *and* C_m) and difference plot (between experimental and calculated data). b) Zoom into the diffraction pattern, hightlighting a superlattice reflection of the C_C phase. c) structure model of the C_C phase, view in the $[001]_c$ direction. d) structure model of the C_C phase, view in the $[010]_c$ direction. In particular, the superstructure in the tiltings of oxygen octahedra can be seen in c) and d).

5. Comparison between Neutron and X-ray diffraction

I) X-rays are scattered at electrons, neutrons are scattered at nuclei

In case of X-ray scattering, the scattering power of an atom (described by the atomic form factor *f*) is proportional to the number of electrons (or: charge density).
Neutrons are scattered at nuclei. Thus the interaction (described by the scattering length b) varies between different isotopes of an element. The ccattering lengths of neighbouring elements in the periodic system can be very different.

implications:

Localisation of light elements next to heavier ones

X-ray diffraction is a powerful tool to determine the positions of heavy atoms, but the localisation of light atoms in the vicinity of much heavier atoms is often difficult or related with high uncertainties. Neutron diffraction is advantageous to localise light atoms such as H, D, Li, C, N, O.

Localisation of neighbouring elements in the periodic table

Neighbouring elements in the periodic table can hardly be distinguished by means of X-ray diffraction. Neutrons are advantageous for such cases: examples: Mn – Fe - Co – Ni or O – N.

Q-dependence of intensities

Since the size of electron clouds is comparable to the wavelength, the atomic form factor depends on $\sin\theta/\lambda$ or *Q*. Therefore the intensities of X-ray reflections decrease significantly for increasing *Q* (increasing scattering angles 2θ).
As the range of the neutron–nuclei–interaction is by orders of magnitude smaller than the wavelengths of thermal neutrons, scattering lengths do not depend on Q. As a consequence, neutron diffraction patterns do not show a decrease of Bragg reflection intensities for higher scattering angles, enabling the analysis of larger Q-ranges. In particular, neutron diffraction is advantageous for the analysis of thermal displacement parameters.

II) neutrons interact weakly with matter

implications:

sample volume

The flux from neutron sources is much lower compared to X-ray tubes or even synchrotrons. In addition, neutrons interact weakly with matter. Therefore, much larger sample amounts are required compared to X-ray diffraction ("grams instead of milligrams"). On the other hand this weak interaction results in much higher penetration depths of neutrons, compared to laboratory X-ray diffractometers. Thus, polycrystalline bulk samples can be investigated. Furthermore, using large sample volumes avoid possible problems due to preferred orientation effects. In this respects, neutron diffraction is typically advantageous for coarse grained materials.

Sample environments

The large penetration depths of neutrons facilitates the usage of sample environments like cryostat, furnaces, magnets, tensile rigs... In general neutron scattering experiments are more versatile applying very high or low temperatures. On the other hand, the small sample volume required for synchrotron studies gives better possibilities for high-pressure experiments.

III) neutrons exhibit a magnetic moment

Though neutrons do not have an electric charge, the internal charge distribution due to its three quarks along with the spin result in a magnetic moment of the neutron.

implications:

magnetic scattering

The interaction between the magnetic moment of the neutron and a possible magnetic moment of an atom results in a magnetic scattering contribution, incidentally in the same order of magnitude as the nuclear scattering contribution. The magnetic scattering contribution can be easily detected by means of neutron diffraction. In synchrotron diffraction studies, possible magnetic scattering events are weaker by several orders of magnitude than the Thomson scattering.

6. Setup of the high-resolution neutron powder diffractometer SPODI at FRM II

The main components of a constant-wavelength neutron powder diffractometer are: source, monochromator, sample and detector (Fig. 8). Between these components collimation systems are installed which have high impact on the instrumental resolution function and the neutron flux.

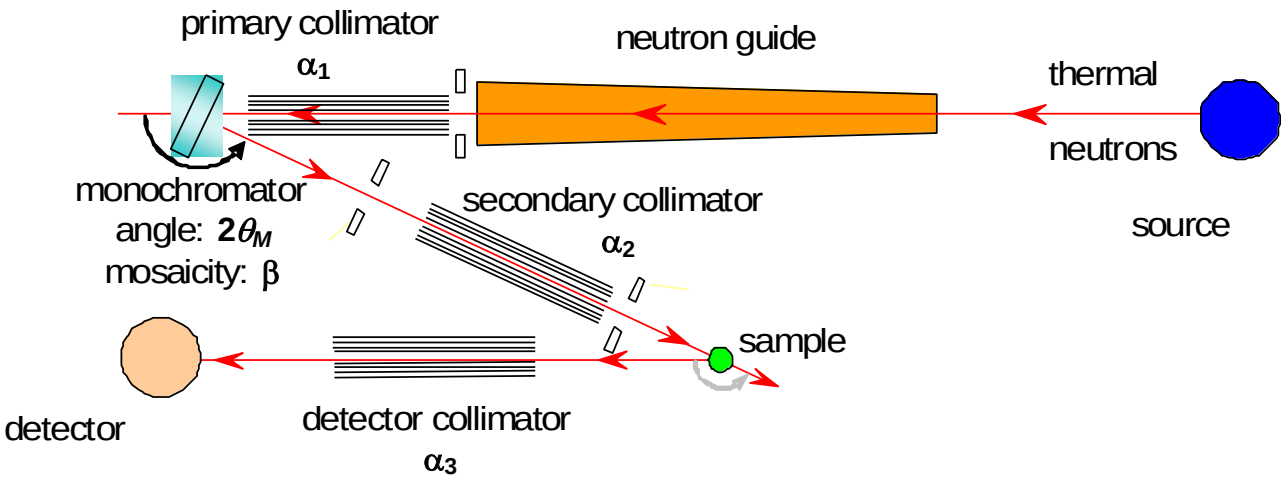

Figure 8: **I**llustration of a typical instrumental layout, introducing the parameters used by Caglioti to describe the instrumental resolution function.

Instrumental resolution function

The instrumental resolution function(of a constant wavelength diffractometer can be expressed by a relation between the full-width at half maximum (FWHM) of the reflections as a function of the scattering angle 2θ. As shown by Calgioti, the instrumental resolution function (of a constant-wavelength powder diffractometer) can be approximated by:

$$FWHM = \sqrt{U\tan^2\theta + V\tan\theta + W}$$

with the Caglioti parameters:

$$U = \frac{4\left(\alpha_1^2\alpha_2^2 + \alpha_1^2\beta^2 + \alpha_2^2\beta^2\right)}{\tan^2\theta_m\left(\alpha_1^2 + \alpha_2^2 + 4\beta^2\right)}$$

$$V = \frac{-4\alpha_2^2\left(\alpha_1^2 + 2\beta^2\right)}{\tan\theta_m\left(\alpha_1^2 + \alpha_2^2 + 4\beta^2\right)}$$

$$W = \frac{\alpha_1^2\alpha_2^2 + \alpha_1^2\alpha_3^2 + \alpha_2^2\alpha_3^2 + 4\beta^2\left(\alpha_2^2 + \alpha_3^2\right)}{\left(\alpha_1^2 + \alpha_2^2 + 4\beta^2\right)}$$

In this approach it is assumed that all components have Gaussian transmission profiles. The resolution function is determined by the horizontal beam divergences α_1, α_2, α_3, the monochromator angle $2\theta_m$ and the mosaicity of the monochromator β (Figure 8). The Caglioti equations help to design an instrument to achieve a designated performance. However, it should be emphasised that in the approximations of Caglioti only the horizontal beam divergences are taken into account, neglecting vertical beam divergences by a vertical focusing monochromator or a vertical divergent neutron guide. Those effects are taken into account by ray-tracing methods, which allow a detailed modelling of the individual components.
The powder diffractometer SPODI has been designed to achieve both high resolution and good profile shape. In its standard configuration (highest resolution mode) SPODI uses a unique very high monochromator take-off angle of 155° along with a large monochromator-to-sample distance of 5 meters. An evacuated beam tube of about 4 m in length is located between the monochromator and the sample which also controls both vertical and horizontal neutron beam divergences at the sample position. Thus the natural neutron beam divergence in horizontal plane is 25’ only.

Monochromator

At constant-wavelength diffractometers, the monochromatisation is perfomed using crystals followings Bragg's equation:

$2d_{hkl}\sin\theta = \lambda$, where the effective transmission band is determined by a derivative

$$\frac{\Delta\lambda}{\lambda} = \Delta\theta_M \cot\theta_M$$

The width of the wavelength band $\Delta\lambda/\lambda$ strongly depends on the monochromator angle $2\theta_m$ and the mosaicity of the monochromator β, i.e $\Delta\theta_m$. Thus these parameters have a major impact on the instrumental resolution function and the flux on the sample.
Typically, the monochromator crystals are installed at a vertical focusing unit of 200 – 300 mm, allowing optimization of the intensity distribution at the sample position with respect to the monochromator – sample distance or the sample height. On the other hand, the vertical beam divergence results in a smearing of the Debye-Scherrer rings along the detector height (this effect depends also on the sample height). At the high-resolution powder diffractometer SPODI, 15 Germanium wafer-stack crystals with a (551)-orientation are used. Different wavelengths between 1.0 Å and 2.6 Å can easily be selected by rotation of the

monochromator unit (without changing the monochromator take-off angle $2\theta_m$), i.e. by selecting different (*hkl)* reflection planes. In general, large wavelengths are advantageous to investigate structures exhibiting large d-values. This is the case for large unit cells, but in particular for magnetic ordering. With decreasing wavelengths, larger Q-values can be achieved. Thus, with lower wavelengths, more reflections can be observed in the same scattering angle range. Low wavelengths are in particular advantageous for the analysis of thermal displacement parameters or static disorder phenomena.

Detector array

At constant-wavelength diffractometers the data are collected in an angle-dispersive manner at equidistant 2θ points. Detector systems based on ^{3}He have been most commonly used due to their very high efficiency. Now, the world wide shortage of ^{3}He demands and promotes the development of alternatives, in particular scintillator based systems.
Classical high-resolution powder diffractometers, such as D2B (ILL), SPODI (FRM II), BT1 (NIST), ECHIDNA (ANSTO) use multidetector/multicollimator systems. The data are collected by ^{3}He tubes while the beam divergence is limited by Soller collimators. Such systems enable high Q-resolution over a broad scattering angle regime, while the resolution does not depend on the sample diameter. On the other hand, a multidetector concept requires a data collection by stepwise positioning of the detector array to collect the full diffraction pattern. Therefore, kinetic measurements are not feasible due to the fact that the sample must not change during the collection of a pattern.
The detector array of SPODI consists of 80 ^{3}He tubes, which are position sensitive in the vertical direction. Thus, two-dimensional raw data are obtained, which allow to rapidly check for sample crystallinity, alignment and possible preferred orientation effects. The conventional diffraction patterns (intensity vs. scattering angle 2θ) are derived from the two-dimensional raw data by integration along the Debye-Scherrer rings.

7. Experiment: Phase- and structure analysis of lead titanate at various temperatures

samples

Lead zirconate titanates $PbZr_{1-x}Ti_xO_3$ („PZT“) exhibit piezo-, pyro- and ferroelectric properties. Piezoelectricity describes the generation of an electric polarisation as a consequence of a mechanical deformation – or the other way round the development of a macroscopic strain by an electric field. The crystallographic condition of piezoelectricity is the lack of an inversion center: as the balance points of negative and positive charge do not coincide the displacements of the ions in the electric field results in a polarization. Pyroelectrticity refers to a spontaneous polarization of a material as a function of temperature. Ferroelectrics are special pyroelectric materials, in which the polarization can be switched by an electric field, resulting in a ferroelectric hysteresis.

The electromechanical properties of $PbZr_{1-x}Ti_xO_3$ can be understood by their phase transformation behaviour. At high temperatures they exhibit the perovskite structure with simple cubic symmetry (space group Pm-3m). Because of its symmetry (inversion center) this phase is not piezoelectric but paraelectric. During cooling, titanium-rich samples undergo a phase transition to a tetragonal phase (space group P4mm). This phase transformation is accompanied by atomic displacements. In particular, the Ti^{4+}/Zr^{4+} are shifted in the opposite direction than O^{2-} ions, resulting in a dipole moment or a spontaneous polarisation. The material exhibits ferroelectric behaviour, with a polar axis in the direction of the pseudocubic c-axis, i.e. $[001]_c$. Zirconium rich samples undergo a phase transition towards a rhombohedral phase (space group R3m) during cooling. In this case, the atomic displacements result in a polar axis in direction $[111]_c$ with respect to the parent pseudocubic lattice. Materials $PbZr_{1-x}Ti_xO_3$ with compositions (Zr/Ti ratios) close to the so called morphotropic phase boundary between rhombohedral and tetragonal phase, show the highest piezoelectric response, i.e. the largest macroscopic strain as a function of the applied electric field. These compositions are therefore most interesting for technological applications. The piezoelectric properties can be modified further by adding doping elements to substitute Pb^{2+} or Ti^{4+}/Zr^{4+} ions.

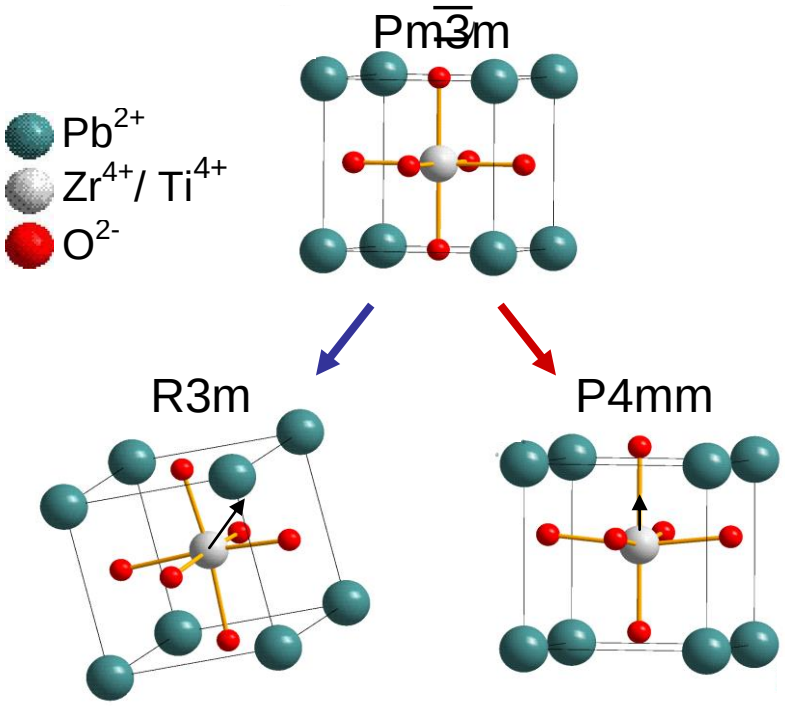

Figure 9: Structure models of the paraelectric cubic phase and the ferroelectric rhombohedral and tetragonal phases.

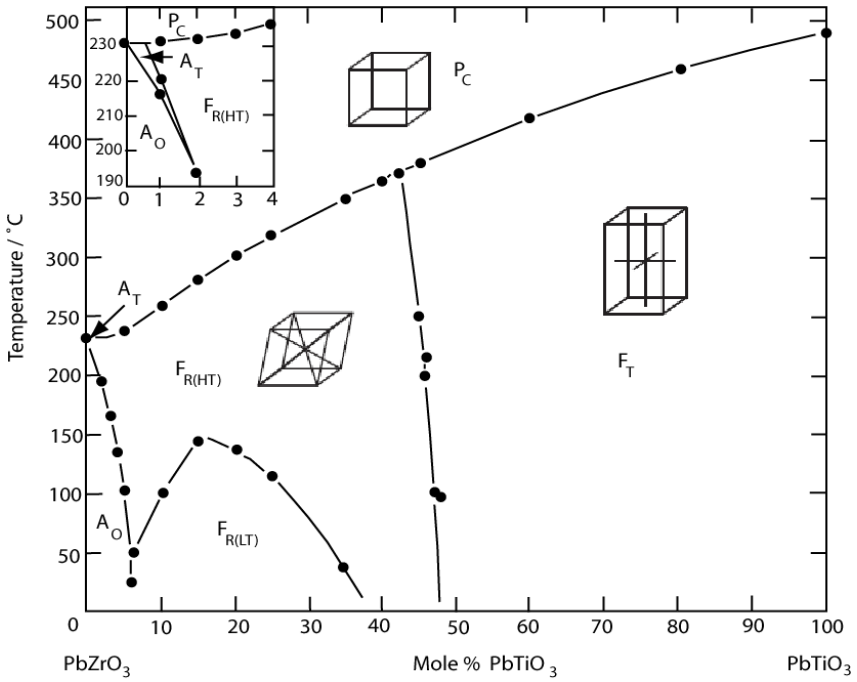

Figure 10: Phase diagram of $PbZr_{1-x}Ti_xO_3$, illustrating regions of phase stability for paraelectric cubic phase P_C, ferroelectric rhomboedral phases $F_{R(HT)}$ (= high temperature) and $F_{R(LT)}$ (= low temperature) and ferroelectric tetragonal phase F_T. From B. Jaffe, W. R. Cook, H. Jaffe, Piezoelectric Ceramics and Related Issues, Academic Press, London, 1971.

$PbZr_{1-x}Ti_xO_3$, find extensive applications

- transformation from mechanical in electric energy: ignition elements, lighters
- transformation from electric in mechanical energy (actuators): fuel injectors, loudspeakers, sonar transducers, active control of vibration, ink printers
- transformation from mechanical force in an electric signal (sensors): strain gauges, microphones
- data storage, information technology: capacitors, F-RAM

Experiment

In the frame of the practical course, the temperature-dependent phase transformation behavior of a $PbZr_{1-x}Ti_xO_3$ with a composition on the tetragonal side should be investigated. Diffraction patterns at different temperature steps between room temperature and 600 °C will be collected with a vacuum high-temperature furnace. The structural changes at different temperatures will be investigated by an analysis of the lattice parameters. Based on the experimental data, the relations between the structural changes and the corresponding physical properties can be discussed.

Following experimental procedures will be carried out

- sample preparation, filling the sample material into a sample can, adjustment of the sample stick, installation of the sample stick into the furnace
- short test measurement to check the sample adjustment and data quality
- editing a program to run the data collection at various temperatures and starting the scans
- data reduction: Derivation of diffraction patterns from the two-dimensional raw data
- data analysis: analysis of the lattice parameter changes as a function of temperature
- discussing the results with respect to structure – properties relationships

Literature

[1] V. K. Pecharsky, P. Y. Zavalij, Fundamentals of Powder Diffraction and structural Characterisation of Materials (2003).
[2] G. L. Squires, Introduction to the Theory of Thermal Neutron Scattering, Dover Reprints (1978).
[3] C. Kittel, Einführung in die Festkörperphysik, 10. Edition, Oldenbourg (1993).
[4] H. Dachs, Neutron Diffraction, Springer Verlag (1978).
[5] H. Ibach und H. Lüth, Festkörperphysik, Einführung in die Grundlagen, 6. Edition, Springer
Verlag (2002).
[6] J.R.D. Copley, The Fundamentals of Neutron Powder Diffraction (2001), http://www.nist.gov/public_affairs/practiceguides/SP960-2.pdf.
[7] A. D. Krawitz, Introduction to Diffraction in Materials Science and Engineering.
[8] W. Kleber, Einführung in die Kristallographie, Oldenbourg (1998).

Contact

SPODI

Web: http://www.frm2.tum.de/wissenschaftliche-nutzung/diffraktion/spodi/index.html

Dr. Markus Hoelzel

Forschungsneutronenquelle Heinz Maier-Leibnitz (FRM II)
Technische Universität München
Phone: 089/289-14314
e-Mail: markus.hoelzel@frm2.tum.de

Dr. Anatoliy Senyshyn

Forschungsneutronenquelle Heinz Maier-Leibnitz (FRM II)
Technische Universität München

Phone: 089/289-14316
e-Mail: anatoliy.senyshyn@frm2.tum.de

Dr. Volodymyr Baran

Forschungsneutronenquelle Heinz Maier-Leibnitz (FRM II)
Technische Universität München

Phone: 089/289-14373
e-Mail: oleksandr.dolotko@frm2.tum.de

Dr. Martin J. Mühlbauer

Institut für Angewandte Materialien (IAM)
Karlsruher Institut für Technologie (KIT)

Phone: 089/289-14373
e-Mail: martin.mühlbauer@frm2.tum.de